


Even-odd parity transition in strongly correlated locally noncentrosymmetric superconductors: Application to CeRh₂As₂

Kosuke Nogaki * and Youichi Yanase

Department of Physics, Kyoto University, Kyoto 606-8502, Japan



(Received 8 June 2022; revised 7 September 2022; accepted 8 September 2022; published 27 September 2022)

The discovery of the multiple H - T phase diagram of CeRh₂As₂ offers a new route to designing topological superconductors. Although weak-coupling theories explain the experimental phase diagram qualitatively, a quantitative discrepancy between them has discouraged a conclusive interpretation. In this Letter, we thoroughly study the effect of the Coulomb interaction and the phase diagrams of locally noncentrosymmetric superconductors. We reveal an even-odd parity transition and the enhancement of the parity transition field in strongly correlated superconductors, and an issue of CeRh₂As₂ is resolved.

DOI: [10.1103/PhysRevB.106.L100504](https://doi.org/10.1103/PhysRevB.106.L100504)

Introduction. Searching for odd-parity superconductors has been a central issue in designing topological materials [1–4]. Due to Fermi statistics, odd-parity superconductors are classified into spin-triplet superconductors within the theory by Bardeen, Cooper, and Schrieffer (BCS) [5], which explains various phenomena of superconductivity. In topological science, this constraint on Cooper pairs has led to the renewed interest in uncommon spin-triplet superconductors such as UPt₃ [6–9], UCoGe [10–12], and UTe₂ [13–16]. However, some internal degrees of freedom of Cooper pairs are overlooked in the canonical BCS theory.

Recently, the local noncentrosymmetry in superconductors has attracted much attention and shed light on the sublattice degrees of freedom in Cooper pairs [17–31]. Interestingly, a sublattice antisymmetric Cooper pair is allowed, leading to an odd-parity superconducting state without spin-triplet pairs. Therefore, sublattice degrees of freedom pave a new way to design topological odd-parity superconductors based on pairing in an ordinary spin-singlet channel [22,32]. In the high-magnetic-field phase of locally noncentrosymmetric superconductors, the sublattice antisymmetric superconducting state is theoretically predicted to be thermodynamically stable, and is called the pair-density-wave (PDW) state [19].

The discovery of the two superconducting phases in the H - T phase diagram of CeRh₂As₂ [33] has focused attention on the sublattice degrees of freedom in superconductors [32–46]. In fact, due to the two-sublattice crystalline structure of CeRh₂As₂, the inversion symmetry is locally broken at the Ce site but globally preserved [33]. The qualitative similarity of the phase diagrams between the weak-coupling theory [19,33] and experiment [33,40] strongly suggests an essential role of local inversion symmetry breaking in CeRh₂As₂, and the two superconducting phases were interpreted based on the even-odd parity transition within the superconducting state [33,40].

In contrast to the preceding argument, there are two issues regarding the nature of CeRh₂As₂. First, the micro-

scopic mechanism of superconductivity in CeRh₂As₂ remains unsolved. The unconventional superconductivity mediated by quantum critical fluctuations is studied in this Letter. Second, the parity transition field of CeRh₂As₂ significantly exceeds the Pauli-Clogston-Chandrasekhar limit and is larger than the prediction of weak-coupling theory by a factor of five [19,33]. Although two scenarios have been proposed within the weak-coupling theory [44,45], we try to resolve the issue by verifying an intrinsic phase diagram of strongly correlated locally noncentrosymmetric superconductors.

To tackle the above-mentioned problems, we focus on the electronic correlation effect of Ce f electrons, which have a localized character. Indeed, the large electronic specific heat coefficient $\gamma \sim 1000$ mJ/mol K² supports the presence of heavy-fermion bands near the Fermi level, and non-Fermi-liquid behaviors suggest quantum criticality in CeRh₂As₂ [33,37,39]. These experimental observations indicate that the Coulomb interaction crucially impacts the electronic state of CeRh₂As₂. Hence, theoretical studies of strong correlation effects in locally noncentrosymmetric superconductors have been desired.

In this Letter, we conduct a thorough study on quantum critical multipole fluctuations, the resulting superconductivity, and the superconducting phase diagrams of locally noncentrosymmetric strongly correlated electron systems. To clarify these properties, the fluctuation exchange (FLEX) approximation which appropriately reproduces the critical behaviors of self-consistent renormalization theory [47] is adopted. In the FLEX scheme, the Green function and the self-energy depend on each other, and therefore the retardation effect, quasiparticle scattering, and internal field are taken into account (see Supplemental Material Sec. S1 [48]). Theoretical results are compared with the superconducting phase diagrams of CeRh₂As₂, and the origin of superconductivity is discussed. As a result, the XY -type antiferromagnetic fluctuation consistent with nuclear magnetic resonance (NMR) [39] and superconductivity with a dominant $d_{x^2-y^2}$ -wave pairing are revealed, and the obtained enhanced parity transition field resolves the issue of the phase diagram in CeRh₂As₂.

*nogaki.kosuke.83v@st.kyoto-u.ac.jp

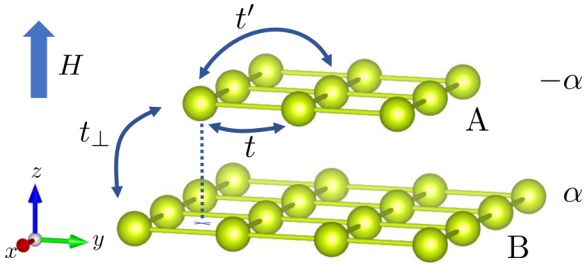


FIG. 1. Schematic figure of the bilayer Rashba-Hubbard model. Yellow circles represent the Ce atoms of CeRh_2As_2 . We introduce first- and second-neighbor intralayer hopping integrals. We also introduce an interlayer hopping integral as t_\perp . The staggered Rashba-type antisymmetric spin-orbit coupling is included in the model as it arises from the asymmetric potential by Rh_2As_2 layers. The magnetic field is applied parallel to the z axis.

Bilayer Rashba-Hubbard model. We focus on the low-energy coherent heavy-fermion band and construct the bilayer Rashba-Hubbard model, in which Coulomb correlation and spin-orbit coupling are taken into account [49,50]. Note that all parameters of our model are renormalized through the Kondo effect. The model is given by

$$\hat{H} = \sum_{\mathbf{k}} \varphi^\dagger(\mathbf{k}) \mathcal{H}_0(\mathbf{k}) \varphi(\mathbf{k}) + U \sum_{i,\sigma} n_{i\uparrow\sigma} n_{i\downarrow\sigma}, \quad (1)$$

where U is the on-site Coulomb repulsion, $\mathcal{H}_0(\mathbf{k}) = \varepsilon(\mathbf{k}) s_0 \otimes \sigma_0 + \alpha \mathbf{g}(\mathbf{k}) \cdot \mathbf{s} \otimes \sigma_z - \mu_B H s_z \otimes \sigma_0 + \tilde{t}_\perp(\mathbf{k}) s_0 \otimes \sigma_+ + \tilde{t}_\perp(-\mathbf{k}) s_0 \otimes \sigma_-$, $\varphi(\mathbf{k}) = (c_{k\uparrow A}, c_{k\downarrow A}, c_{k\uparrow B}, c_{k\downarrow B})^\top$, and $c_{k s \sigma}$ ($c_{k s \sigma}^\dagger$) is an annihilation (creation) operator for an electron with momentum \mathbf{k} , spin s , and sublattice $\sigma \in \{A, B\}$ (Fig. 1). Here, s_μ and σ_μ consisting of a 2×2 unit matrix and three Pauli matrices represent spin and sublattice degrees of freedom, respectively.¹ The first term of \mathcal{H}_0 represents intralayer hopping including the chemical potential and is given by $\varepsilon(\mathbf{k}) = -2t(\cos k_x + \cos k_y) + 4t' \cos k_x \cos k_y - \mu$. The vector $\mathbf{g}(\mathbf{k})$ describes the Rashba-type antisymmetric spin-orbit coupling given by $\mathbf{g}(\mathbf{k}) = [-\partial \varepsilon(\mathbf{k}) / \partial k_y, \partial \varepsilon(\mathbf{k}) / \partial k_x, 0]$, and H represents the Zeeman magnetic field parallel to the z axis. The last two terms of \mathcal{H}_0 describe interlayer hopping given as $\tilde{t}_\perp(\mathbf{k}) = t_\perp(1 + e^{-ik_x})(1 + e^{-ik_y})$. This model is a straightforward extension of the Rashba-Hubbard model for globally inversion-asymmetric strongly correlated electron systems [51–63]. Hereafter, we set $t' = 0.3$, $t_\perp = 0.1$, $\mu_B = 1$, and $U = 3.9$ with a unit of energy $t = 1$ and determine the chemical potential so that the electron density per site n is 0.85. In the present numerical study, we use 64×64 \mathbf{k} meshes, and 16384, 8192, or 4096 Matsubara frequencies for $T = 0.004$, $0.004 < T < 0.01$, or $0.01 \leq T$, respectively. By comparing with the quantum Monte Carlo method, the FLEX approximation was confirmed as a reliable method within the intermediate-coupling region in which the Coulomb interaction U is smaller than half of the bandwidth W , namely, the condition for justification of the FLEX approximation is $U/W \lesssim 0.5$ [64–68]. Our choice of model parameters satisfies this condition and the FLEX

¹ μ runs over $\{0, x, y, z\}$, and σ_\pm are given by $(\sigma_x \pm i\sigma_y)/2$.

TABLE I. Classification of the multipole operators in the bilayer Rashba-Hubbard model. Here, $\hat{s}_\pm = (\hat{s}_x \pm i\hat{s}_y)/\sqrt{2}$ are ladder operators for spin. E (O) represents the even-parity (odd-parity) multipole operators. C, L, and T represent charge, longitudinal spin, and transverse spin operators, respectively. $\hat{\sigma}_0$ and $\hat{\sigma}_z$ ($\hat{\sigma}_x$ and $\hat{\sigma}_y$) are intrasublattice (intersublattice) operators.

$\hat{\mathcal{O}}$	$\hat{\sigma}_0$	$\hat{\sigma}_x$	$\hat{\sigma}_y$	$\hat{\sigma}_z$
\hat{s}_0	E C intra	E C inter	O C inter	O C intra
\hat{s}_z	E L intra	E L inter	O L inter	O L intra
\hat{s}_\pm	E T intra	E T inter	O T inter	O T intra

approximation is expected to give a good description of strongly correlated superconductors in this case.

Multipole susceptibility. First, we discuss quantum critical multipole fluctuations. A dynamical susceptibility tensor is given by the generalized susceptibility as

$$\chi_{\hat{\mathcal{O}}}(\mathbf{q}, i\nu_n) = \sum_{\xi_1 \xi_2 \xi_3 \xi_4} \hat{\mathcal{O}}_{\xi_1 \xi_2} \chi_{\xi_2 \xi_1 \xi_3 \xi_4}(\mathbf{q}, i\nu_n) \hat{\mathcal{O}}_{\xi_3 \xi_4}, \quad (2)$$

where $i\nu_n$ are bosonic Matsubara frequencies and ξ is abbreviated notation for $\xi = (s, \sigma)$. The operators $\hat{\mathcal{O}}$ are (extended) multipole operators as $\hat{\mathcal{O}} = \hat{s} \otimes \hat{\sigma}$ [69–71], and classified into even-parity (odd-parity) multipoles for $\hat{\sigma}_0, \hat{\sigma}_x$ ($\hat{\sigma}_y, \hat{\sigma}_z$). In Table I, we summarize the classification of multipole operators in our system. We adopt the normalization convention $\text{tr}[\hat{\mathcal{O}}^\dagger \hat{\mathcal{O}}] = 1$, and therefore operators are represented by the Pauli matrices as $\hat{s}_\mu = s_\mu / \sqrt{2}$ and $\hat{\sigma}_\mu = \sigma_\mu / \sqrt{2}$.

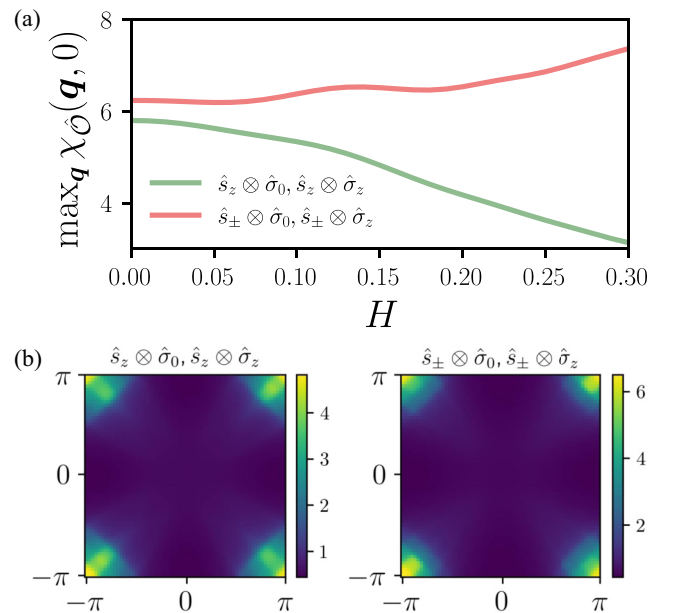


FIG. 2. (a) The magnetic field dependence of static multipole fluctuations. The maxima of the longitudinal and transverse magnetic susceptibilities are shown. Note that the even-parity and odd-parity multipole fluctuations are nearly degenerate. We assume $\alpha/t_\perp = 2$ and $T = 0.01$. (b) The momentum dependence of longitudinal magnetic susceptibility (left) and transverse magnetic susceptibility (right) at $H = 0.15$.

In Fig. 2(a), the magnetic field dependence of the maximum of transverse and longitudinal magnetic susceptibilities is shown. We see that the transverse (longitudinal) susceptibility is enhanced (reduced) by the magnetic field. Note that the even-parity magnetic multipole fluctuation for $s \otimes \sigma_0$ and the odd-parity magnetic multipole fluctuation for $s \otimes \sigma_z$ are nearly degenerate, while the odd-parity multipole is slightly favored. Other multipole susceptibilities are negligibly small. From Fig. 2(b), both transverse and longitudinal magnetic susceptibilities show the peak structure around $\mathbf{Q} = (\pi, \pi)$, and thus an antiferromagnetic spin fluctuation develops in the system. The momentum dependence is not qualitatively affected by the magnetic field. Therefore, we presume a dominant XY -type antiferromagnetic fluctuation,² which is consistent with the observation in CeRh_2As_2 by the NMR measurement [39]. We confirmed that the behaviors of the multipole susceptibility do not qualitatively depend on the strength of spin-orbit coupling α/t_\perp (see Supplemental Material Sec. S2) [48].

Superconductivity. To investigate superconductivity, we adopt the linearized Eliashberg equation which is given by

$$\lambda \Delta_{\xi\xi'}(k) = \frac{T}{N} \sum_{k'} \Gamma_{\xi\xi_1\xi_2\xi'}^a(k-k') F_{\xi_1\xi_2}(k), \quad (3)$$

$$F_{\xi_1\xi_2}(k) = G_{\xi_1\xi_3}(k') \Delta_{\xi_3\xi_4}(k') G_{\xi_2\xi_4}(-k'), \quad (4)$$

where Δ is the gap function and Γ^a is the particle-particle channel irreducible vertex function. Here, we adopted abbreviated notation $k = (\mathbf{k}, i\omega_n)$. With the power method, we numerically evaluate λ , eigenvalues of the linearized Eliashberg equation and determine the critical temperature T_c from the criterion $\lambda = 1$.

The crystalline space group of CeRh_2As_2 is $P4/nmm$ (No. 129), and therefore the point group is D_{4h} . Since we introduce the magnetic field parallel to the z axis, some symmetry operations are prohibited, and the point group reduces to C_{4h} . Hence, the superconducting gap functions are classified based on irreducible representations of C_{4h} . Using conventional notation, we decompose the superconducting gap functions into the spin-singlet component and spin-triplet component,

$$\Delta^{\sigma\sigma'}(\mathbf{k}) = \{\psi^{\sigma\sigma'}(\mathbf{k}) + \mathbf{d}^{\sigma\sigma'}(\mathbf{k}) \cdot \mathbf{s}\} i s_y, \quad (5)$$

for the intrasublattice and intersublattice pairing channels.³ Here, $\psi^{\text{AA}}(\mathbf{k})$ [$\psi^{\text{AB}}(\mathbf{k})$] represents an intrasublattice (intersublattice) spin-singlet order parameter, while $\mathbf{d}^{\text{AA}}(\mathbf{k})$ [$\mathbf{d}^{\text{AB}}(\mathbf{k})$] is an intrasublattice (intersublattice) spin-triplet order parameter. In the following calculations, the order parameters of intersublattice pairing are negligibly small. The basis functions of the intrasublattice order parameter for each irreducible representation of C_{4h} are summarized in Table II.

In Fig. 3(a), the eigenvalues of the Eliashberg equation for each irreducible representation are shown (see Supplemental Material Secs. S3 and S4) [48]. The B_g and B_u representations are dominant. From the momentum dependence displayed

TABLE II. The basis functions for the intrasublattice superconducting order parameter. IR represents the irreducible representations of the point group C_{4h} . We take into account the time-reversal symmetry breaking under the magnetic field, and the degeneracy of the $E_{g/u}$ states is lifted. Thus, we distinguish them as $E_{g/u}^1$ and $E_{g/u}^2$. Note that the spin-singlet component $\psi(\mathbf{k})$ and spin-triplet in-plane component $d_{x,y}(\mathbf{k})$ for the E representations are prohibited due to the C_2^z rotation symmetry.

IR	$\psi(\mathbf{k})$	$\mathbf{d}(\mathbf{k})$
A_g, A_u	$1, k_x k_y (k_x^2 - k_y^2)$	$k_x \hat{x} + k_y \hat{y}, k_y \hat{x} - k_x \hat{y}$
B_g, B_u	$k_x k_y, k_x^2 - k_y^2$	$k_x \hat{x} - k_y \hat{y}, k_y \hat{x} + k_x \hat{y}$
E_g^1, E_u^1	0	$(k_x + ik_y) \hat{z}$
E_g^2, E_u^2	0	$(k_x - ik_y) \hat{z}$

in Fig. 3(b), both of these states contain spin-singlet $d_{x^2-y^2}$ -wave dominant pairing as well as spin-triplet subdominant pairing with p -wave symmetry. These unconventional Cooper pairs are stabilized by the antiferromagnetic fluctuations and spin-orbit coupling and not significantly changed against the magnetic field.

With almost the same momentum dependence, the different sublattice structures of the gap functions distinguish the B_g and B_u representations. In the even-parity B_g representation, the spin-singlet (spin-triplet) gap function has the same (opposite) sign between the sublattices A and B, as $\psi^{\text{AA}}(\mathbf{k}) = \psi^{\text{BB}}(\mathbf{k})$ and $\mathbf{d}^{\text{AA}}(\mathbf{k}) = -\mathbf{d}^{\text{BB}}(\mathbf{k})$. On the other hand, $\psi^{\text{AA}}(\mathbf{k}) = -\psi^{\text{BB}}(\mathbf{k})$ and $\mathbf{d}^{\text{AA}}(\mathbf{k}) = \mathbf{d}^{\text{BB}}(\mathbf{k})$ in the odd-parity B_u representation. Therefore, the B_g and B_u representations correspond to the BCS and PDW states predicted in the weak-coupling theory [19]. As shown in Fig. 3(a), eigenvalues of the Eliashberg equation for both B_g and B_u

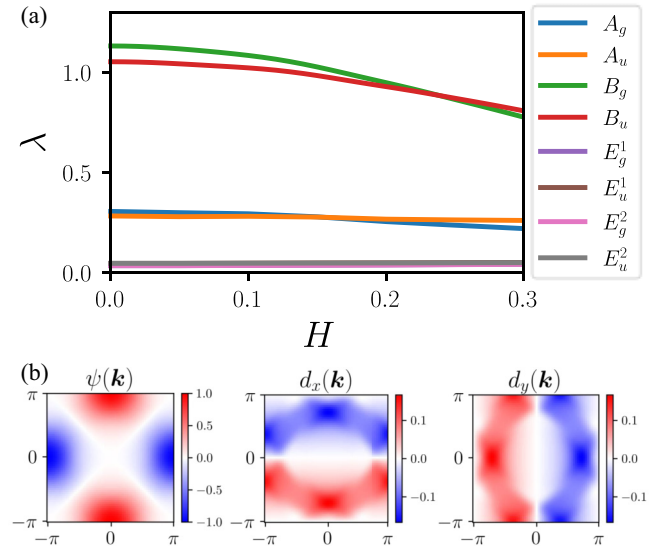


FIG. 3. (a) The magnetic field dependence of eigenvalues of the Eliashberg equation for each irreducible representation. We assume $\alpha/t_\perp = 2$ and $T = 0.01$. (b) The momentum dependence of intrasublattice spin-singlet and spin-triplet gap functions, $\psi^{\text{AA}}(\mathbf{k})$ and $\mathbf{d}^{\text{AA}}(\mathbf{k})$, of the B_g representation for $H = 0.15$. Note that $d_z^{\sigma\sigma}(\mathbf{k}) = 0$. Results for the B_u representation are almost the same as the figures.

²An XY -type fluctuation means that transverse fluctuations dominate over longitudinal ones in the paramagnetic state.

³In our system, the intrasublattice pairing corresponds to the intralayer pairing while the intersublattice pairing corresponds to the interlayer pairing.

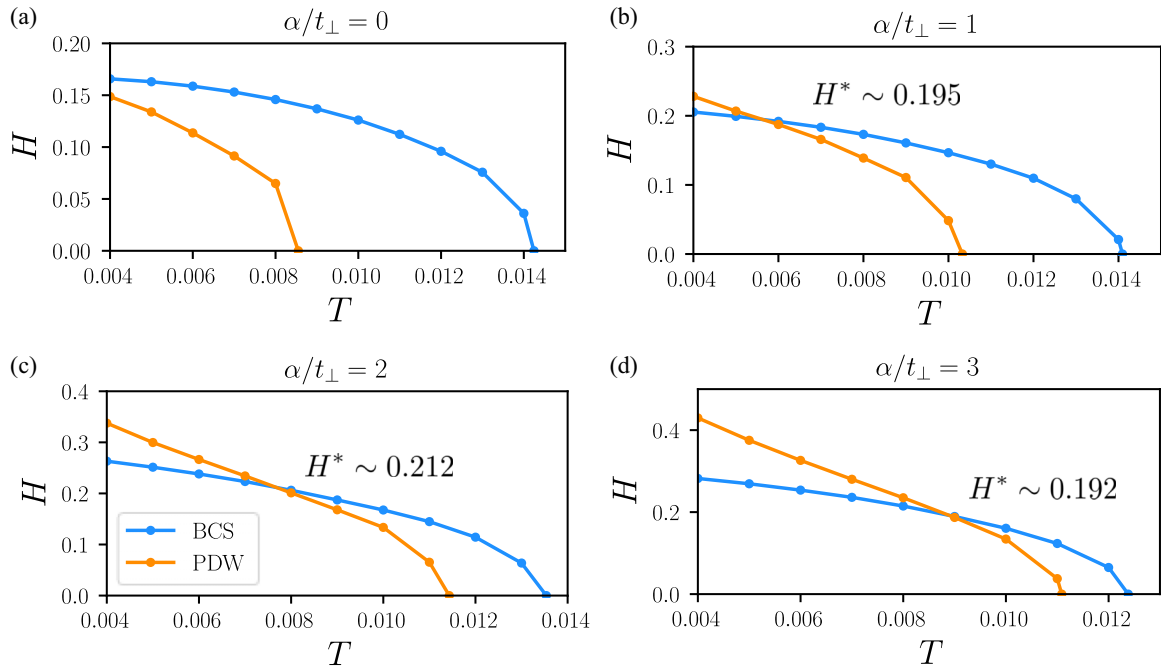


FIG. 4. (a)–(d) H - T phase diagrams of the bilayer Rashba-Hubbard model for $\alpha/t_{\perp} = 0, 1, 2, 3$. We show the superconducting transition lines of the even-parity B_g and odd-parity B_u states, on which eigenvalues of the Eliashberg equation become unity. The BCS and PDW states correspond to the B_g and B_u superconducting phases, respectively. H^* denotes the magnetic field at the parity transition point.

representations are weakened by the magnetic field due to the Pauli depairing effect. However, the B_u state is more robust compared with the B_g state, and therefore at $H = 0.24$ the parity transition from the even-parity B_g state to the odd-parity B_u state occurs. The transition can be understood from the viewpoint of the intrinsic magnetic response of these states. Indeed, the B_g state is Pauli limited, but the B_u state mostly avoids the Pauli limiting because the magnetic susceptibility does not decrease through the superconducting transition [18,30].

Phase diagram. Let us discuss the H - T phase diagram of the bilayer Rashba-Hubbard model. In Figs. 4(a)–4(d), we show the phase diagrams for $\alpha/t_{\perp} = 0, 1, 2$, and 3 , which is known as a control parameter of local noncentrosymmetry [18].⁴ We show the superconducting transition lines of the B_g and B_u states, which correspond to the BCS and PDW states as mentioned before.

From the obtained phase diagrams, the zero-field superconducting transition temperature T_c and the magnetic field at the parity transition point H^* are estimated as $(T_c, H^*) = (0.0141, 0.195)$, $(0.0135, 0.212)$, and $(0.0124, 0.192)$ for $\alpha/t_{\perp} = 1, 2$, and 3 , respectively. From these estimations, we evaluate H^* with a unit of T_c ,

$$\frac{H^*}{T_c} = \begin{cases} 13.8 & (\alpha/t_{\perp} = 1), \\ 15.7 & (\alpha/t_{\perp} = 2), \\ 15.5 & (\alpha/t_{\perp} = 3). \end{cases} \quad (6)$$

⁴While the case $\alpha/t_{\perp} = 0$ corresponds to the bilayer system without spin-orbit coupling, for $\alpha/t_{\perp} = \infty$ the system is equivalent to a set of monolayer systems with Rashba-type spin-orbit coupling [18].

Thus, we conclude that the parity transition fields scaled by the transition temperature are approximately $H^*/T_c \simeq 15$ and universal against a variation of α/t_{\perp} . Although a much smaller value $H^*/T_c \simeq 2$ was predicted by the mean-field theory [19], in CeRh_2As_2 the experimental values $H^* \simeq 3.9$ T and $T_c \simeq 0.26$ K lead $(H^*/T_c)_{\text{exp}} \simeq 10$ [33]. Hence, our theoretical result is quantitatively consistent with the phase diagram of CeRh_2As_2 and resolves the discrepancy between the weak-coupling theory and experiment.

Now we discuss the origin of the enhancement in the parity transition field H^* . First, a possible origin is the nonsymmorphic crystalline symmetry as proposed in Ref. [45]. Actually, an indicator of local noncentrosymmetry $\alpha/\tilde{t}_{\perp}(\mathbf{k})$ diverges at the Brillouin zone faces in nonsymmorphic crystals because of $\tilde{t}_{\perp}(\mathbf{k}_{\text{face}}) = 0$, and therefore the effect of the spin-orbit coupling is more essential than the symmorphic case [45,72]. However, our analysis of the bilayer Rashba-Hubbard model does not support this possibility, because the ratio H^*/T_c is universal against a variation of α/t_{\perp} . Second, we may expect that the spin-triplet component in the gap function changes the spin state of Cooper pairs and increases H^* . However, this is also unlikely because we observe a strong dependence on α/t_{\perp} of the parity mixing parameter r (Fig. 5), which is defined as

$$r = \frac{\max_{\mathbf{k}} |\mathbf{d}^{\text{AA}}(\mathbf{k})|^2}{\max_{\mathbf{k}} |\psi^{\text{AA}}(\mathbf{k})|^2}. \quad (7)$$

From Eq. (6) and Fig. 5, we find that H^*/T_c and r are almost uncorrelated. Third, we rule out the field dependence of the effective interaction as the main origin. In the bilayer Rashba-Hubbard model, the effective pairing interaction is field dependent because of the field-enhanced magnetic anisotropy (see Fig. 2). Figure 6 shows eigenvalues of the Eliashberg

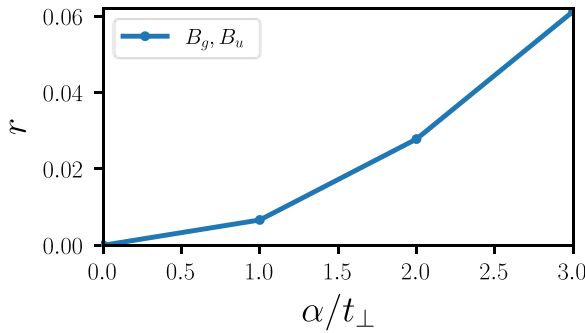


FIG. 5. The parity mixing parameter r as a function of α/t_{\perp} . The values for the B_g and B_u representations are nearly the same. We assume $T = 0.01$ and $H = 0.15$.

equation with and without the field dependence of magnetic anisotropy,⁵ and we find that the field-enhanced magnetic anisotropy weakens the superconducting instabilities. However, the parity transition field H^* is hardly affected. Thus, field-enhanced magnetic anisotropy is also irrelevant for the enhancement of H^* . We conclude from these considerations that a large parity transition field consistent with CeRh_2As_2 is due to the internal field arising from the quantum critical antiferromagnetic fluctuation. Near the antiferromagnetic critical point, the spin correlation between electrons significantly develops and electrons give an internal field to other electrons. In our system, the external Zeeman field applied to an electron is screened by the surrounding electrons, and therefore, the scale of magnetic fields is remarkably increased [73]. This is consistent with the large upper critical fields of CeRh_2As_2 which significantly exceeds the Pauli-Clogston-Chandrasekhar limit even for the in-plane direction [33].

Conclusion. We investigated the nature of quantum critical multipole fluctuation and superconductivity in the bi-

⁵To investigate the effect of the field-induced change of effective interaction, we solve the Eliashberg equation with the zero-field vertex functions while the Green function at $H \neq 0$ are adopted. The eigenvalue without the field-enhanced magnetic anisotropy λ^{iso} is defined by the equations $\lambda^{\text{iso}} \Delta_{\xi\xi'}(k) = \frac{T}{N} \sum_{k'} \Gamma_{\xi\xi_1\xi_2\xi'}^{a,H=0}(k-k') F_{\xi_1\xi_2}^{H \neq 0}(k)$ and $F_{\xi_1\xi_2}^{H \neq 0}(k) = G_{\xi_1\xi_3}^{H \neq 0}(k') \Delta_{\xi_3\xi_4}(k') G_{\xi_2\xi_4}^{H \neq 0}(-k')$.

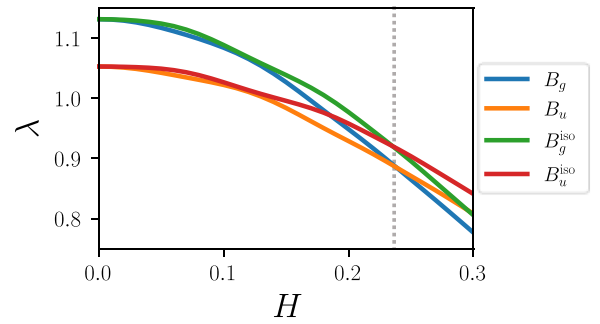


FIG. 6. The magnetic field dependence of eigenvalues of the Eliashberg equation for the B_g and B_u representations. B_g^{iso} and B_u^{iso} represent the eigenvalues without the field-enhanced magnetic anisotropy. The parity transition points are indicated by the gray dashed line. We assume $\alpha/t_{\perp} = 2$ and $T = 0.01$.

layer Rashba-Hubbard model, a minimal model of locally noncentrosymmetric strongly correlated electron systems. Experimental observations in a recently discovered superconductor CeRh_2As_2 [33] were discussed. The XY -type antiferromagnetic fluctuations are shown consistent with the NMR study [39], and the applied magnetic field along the z axis enhances the fluctuations. Due to the critical antiferromagnetic fluctuation, superconductivity with dominant $d_{x^2-y^2}$ -wave pairing and subdominant p -wave pairing is stabilized, and the two superconducting phases with different space inversion parity appear in the H - T phase diagram, consistent with CeRh_2As_2 . The parity transition field is enhanced by the quantum critical fluctuation, and the obtained value is in quantitative agreement with the experimental value. These results support the parity transition in the superconducting state of CeRh_2As_2 [33] and indicate topological superconductivity [32]. Our theory not only solves the issues of CeRh_2As_2 but also elucidates general behaviors of the family of locally noncentrosymmetric strongly correlated superconductors.

Acknowledgments. The authors are grateful to A. Daido and S. Sumita for fruitful discussions. Some figures in this work were created by using VESTA [74]. This work was supported by JSPS KAKENHI (Grants No. JP18H01178, No. JP18H05227, No. JP20H05159, No. JP21J23007, No. JP21K18145, No. JP22H01181, and No. JP22H04933) and SPIRITS 2020 of Kyoto University.

[1] X.-L. Qi and S.-C. Zhang, Topological insulators and superconductors, *Rev. Mod. Phys.* **83**, 1057 (2011).
 [2] Y. Tanaka, M. Sato, and N. Nagaosa, Symmetry and topology in superconductors odd-frequency pairing and edge states, *J. Phys. Soc. Jpn.* **81**, 011013 (2012).
 [3] M. Sato and S. Fujimoto, Majorana fermions and topology in superconductors, *J. Phys. Soc. Jpn.* **85**, 072001 (2016).
 [4] M. Sato and Y. Ando, Topological superconductors: a review, *Rep. Prog. Phys.* **80**, 076501 (2017).
 [5] J. Bardeen, L. N. Cooper, and J. R. Schrieffer, Theory of superconductivity, *Phys. Rev.* **108**, 1175 (1957).

[6] R. Joynt and L. Taillefer, The superconducting phases of UPt_3 , *Rev. Mod. Phys.* **74**, 235 (2002).
 [7] Y. Tsutsumi, M. Ishikawa, T. Kawakami, T. Mizushima, M. Sato, M. Ichioka, and K. Machida, UPt_3 as a topological crystalline superconductor, *J. Phys. Soc. Jpn.* **82**, 113707 (2013).
 [8] Y. Yanase, Nonsymmorphic Weyl superconductivity in UPt_3 based on E_{2u} representation, *Phys. Rev. B* **94**, 174502 (2016).
 [9] Y. Yanase and K. Shiozaki, Möbius topological superconductivity in UPt_3 , *Phys. Rev. B* **95**, 224514 (2017).
 [10] D. Aoki and J. Flouquet, Superconductivity and ferromagnetic quantum criticality in uranium compounds, *J. Phys. Soc. Jpn.* **83**, 061011 (2014).

- [11] D. Aoki, K. Ishida, and J. Flouquet, Review of U-based ferromagnetic superconductors: Comparison between UGe_2 , URhGe , and UCoGe , *J. Phys. Soc. Jpn.* **88**, 022001 (2019).
- [12] A. Daido, T. Yoshida, and Y. Yanase, \mathbb{Z}_4 Topological Superconductivity in UCoGe , *Phys. Rev. Lett.* **122**, 227001 (2019).
- [13] J. Ishizuka, S. Sumita, A. Daido, and Y. Yanase, Insulator-Metal Transition and Topological Superconductivity in UTe_2 From a First-Principles Calculation, *Phys. Rev. Lett.* **123**, 217001 (2019).
- [14] J. Ishizuka and Y. Yanase, Periodic Anderson model for magnetism and superconductivity in UTe_2 , *Phys. Rev. B* **103**, 094504 (2021).
- [15] D. Aoki, J.-P. Brison, J. Flouquet, K. Ishida, G. Knebel, Y. Tokunaga, and Y. Yanase, Unconventional superconductivity in UTe_2 , *J. Phys.: Condens. Matter* **34**, 243002 (2022).
- [16] H. Fujibayashi, G. Nakamine, K. Kinjo, S. Kitagawa, K. Ishida, Y. Tokunaga, H. Sakai, S. Kambe, A. Nakamura, Y. Shimizu, Y. Homma, D. Li, F. Honda, and D. Aoki, Superconducting order parameter in UTe_2 determined by Knight shift measurement, *J. Phys. Soc. Jpn.* **91**, 043705 (2022).
- [17] M. H. Fischer, F. Loder, and M. Sigrist, Superconductivity and local noncentrosymmetry in crystal lattices, *Phys. Rev. B* **84**, 184533 (2011).
- [18] D. Maruyama, M. Sigrist, and Y. Yanase, Locally noncentrosymmetric superconductivity in multilayer systems, *J. Phys. Soc. Jpn.* **81**, 034702 (2012).
- [19] T. Yoshida, M. Sigrist, and Y. Yanase, Pair-density wave states through spin-orbit coupling in multilayer superconductors, *Phys. Rev. B* **86**, 134514 (2012).
- [20] T. Yoshida, M. Sigrist, and Y. Yanase, Complex-stripe phases induced by staggered Rashba spin-orbit coupling, *J. Phys. Soc. Jpn.* **82**, 074714 (2013).
- [21] T. Yoshida, M. Sigrist, and Y. Yanase, Parity-mixed superconductivity in locally noncentrosymmetric system, *J. Phys. Soc. Jpn.* **83**, 013703 (2014).
- [22] T. Yoshida, M. Sigrist, and Y. Yanase, Topological Crystalline Superconductivity in Locally Noncentrosymmetric Multilayer Superconductors, *Phys. Rev. Lett.* **115**, 027001 (2015).
- [23] Y. Higashi, Y. Nagai, T. Yoshida, Y. Masaki, and Y. Yanase, Robust zero-energy bound states around a pair-density-wave vortex core in locally noncentrosymmetric superconductors, *Phys. Rev. B* **93**, 104529 (2016).
- [24] M. Shimozawa, S. K. Goh, T. Shibauchi, and Y. Matsuda, From Kondo lattices to Kondo superlattices, *Rep. Prog. Phys.* **79**, 074503 (2016).
- [25] S.-L. Wu, K. Sumida, K. Miyamoto, K. Taguchi, T. Yoshikawa, A. Kimura, Y. Ueda, M. Arita, M. Nagao, S. Watauchi, I. Tanaka, and T. Okuda, Direct evidence of hidden local spin polarization in a centrosymmetric superconductor $\text{LaO}_{0.55}\text{F}_{0.45}\text{BiS}_2$, *Nat. Commun.* **8**, 1919 (2017).
- [26] T. Yoshida, A. Daido, Y. Yanase, and N. Kawakami, Fate of Majorana Modes in $\text{CeCoIn}_5/\text{YbCoIn}_5$ superlattices: A Test Bed for the Reduction of Topological Classification, *Phys. Rev. Lett.* **118**, 147001 (2017).
- [27] Y. Nakamura and Y. Yanase, Odd-parity superconductivity in bilayer transition metal dichalcogenides, *Phys. Rev. B* **96**, 054501 (2017).
- [28] K. Gottlieb, C.-Y. Lin, M. Serbyn, W. Zhang, C. L. Smallwood, C. Jozwiak, H. Eisaki, Z. Hussain, A. Vishwanath, and A. Lanzara, Revealing hidden spin-momentum locking in a high-temperature cuprate superconductor, *Science* **362**, 1271 (2018).
- [29] D. Möckli, Y. Yanase, and M. Sigrist, Orbitaly limited pair-density-wave phase of multilayer superconductors, *Phys. Rev. B* **97**, 144508 (2018).
- [30] A. Skurativska, M. Sigrist, and M. H. Fischer, Spin response and topology of a staggered-Rashba superconductor, *Phys. Rev. Res.* **3**, 033133 (2021).
- [31] M. H. Fischer, M. Sigrist, D. F. Agterberg, and Y. Yanase, Superconductivity and local inversion-symmetry breaking, [arXiv:2204.02449](https://arxiv.org/abs/2204.02449).
- [32] K. Nogaki, A. Daido, J. Ishizuka, and Y. Yanase, Topological crystalline superconductivity in locally noncentrosymmetric CeRh_2As_2 , *Phys. Rev. Res.* **3**, L032071 (2021).
- [33] S. Khim, J. F. Landaeta, J. Banda, N. Bannor, M. Brando, P. M. R. Brydon, D. Hafner, R. Kuchler, R. Cardoso-Gil, U. Stockert, A. P. Mackenzie, D. F. Agterberg, C. Geibel, and E. Hassinger, Field-induced transition within the superconducting state of CeRh_2As_2 , *Science* **373**, 1012 (2021).
- [34] A. Pourret and G. Knebel, Driving multiphase superconductivity, *Science* **373**, 962 (2021).
- [35] S.-I. Kimura, J. Sichelschmidt, and S. Khim, Optical study of the electronic structure of locally noncentrosymmetric CeRh_2As_2 , *Phys. Rev. B* **104**, 245116 (2021).
- [36] S. Onishi, U. Stockert, S. Khim, J. Banda, M. Brando, and E. Hassinger, Low-temperature thermal conductivity of the two-phase superconductor CeRh_2As_2 , *Front. Electron. Mater.* **2**, 880579(2022).
- [37] D. Hafner, P. Khanenko, E.-O. Eljaouhari, R. Kuchler, J. Banda, N. Bannor, T. Lühmann, J. F. Landaeta, S. Mishra, I. Sheikin, E. Hassinger, S. Khim, C. Geibel, G. Zwirgagl, and M. Brando, Possible Quadrupole Density Wave in the Superconducting Kondo Lattice CeRh_2As_2 , *Phys. Rev. X* **12**, 011023 (2022).
- [38] M. Kibune, S. Kitagawa, K. Kinjo, S. Ogata, M. Manago, T. Taniguchi, K. Ishida, M. Brando, E. Hassinger, H. Rosner, C. Geibel, and S. Khim, Observation of Antiferromagnetic Order as Odd-Parity Multipoles Inside the Superconducting Phase in CeRh_2As_2 , *Phys. Rev. Lett.* **128**, 057002 (2022).
- [39] S. Kitagawa, M. Kibune, K. Kinjo, M. Manago, T. Taniguchi, K. Ishida, M. Brando, E. Hassinger, C. Geibel, and S. Khim, Two-dimensional XY-type magnetic properties of locally noncentrosymmetric superconductor CeRh_2As_2 , *J. Phys. Soc. Jpn.* **91**, 043702 (2022).
- [40] J. F. Landaeta, P. Khanenko, D. C. Cavanagh, C. Geibel, S. Khim, S. Mishra, I. Sheikin, P. M. R. Brydon, D. F. Agterberg, M. Brando, and E. Hassinger, Field-Angle Dependence Reveals Odd-Parity Superconductivity in CeRh_2As_2 , *Phys. Rev. X* **12**, 031001 (2022).
- [41] E. G. Schertenleib, M. H. Fischer, and M. Sigrist, Unusual H - T phase diagram of CeRh_2As_2 : The role of staggered noncentrosymmetry, *Phys. Rev. Res.* **3**, 023179 (2021).
- [42] D. Möckli and A. Ramires, Two scenarios for superconductivity in CeRh_2As_2 , *Phys. Rev. Res.* **3**, 023204 (2021).
- [43] A. Ptok, K. J. Kapcia, P. T. Jochym, J. Łażewski, A. M. Oleś, and P. Piekarz, Electronic and dynamical properties of CeRh_2As_2 : Role of Rh_2As_2 layers and expected orbital order, *Phys. Rev. B* **104**, L041109 (2021).
- [44] D. Möckli and A. Ramires, Superconductivity in disordered locally noncentrosymmetric materials: An application to CeRh_2As_2 , *Phys. Rev. B* **104**, 134517 (2021).

- [45] D. C. Cavanagh, T. Shishidou, M. Weinert, P. M. R. Brydon, and D. F. Agterberg, Nonsymmorphic symmetry and field-driven odd-parity pairing in CeRh_2As_2 , *Phys. Rev. B* **105**, L020505 (2022).
- [46] T. Hazra and P. Coleman, Triplet pairing mechanisms from Hund's-Kondo models: Applications to UTe_2 and CeRh_2As_2 , [arXiv:2205.13529](https://arxiv.org/abs/2205.13529).
- [47] T. Moriya and K. Ueda, Spin fluctuations and high temperature superconductivity, *Adv. Phys.* **49**, 555 (2000).
- [48] See Supplemental Material at <http://link.aps.org/supplemental/10.1103/PhysRevB.106.L100504> for a detailed description of the FLEX approximation (Sec. S1), for the multipole susceptibility for different α/t_\perp (Sec. S2), and for the eigenvalues of the Eliashberg equation for different α/t_\perp (Secs. S3 and S4).
- [49] L. Craco, Correlated nature of hybrid s -wave superconducting and Rashba lattices, *Phys. Rev. B* **104**, 064509 (2021).
- [50] X. Lu and D. S en echal, Spin texture in a bilayer high-temperature cuprate superconductor, *Phys. Rev. B* **104**, 024502 (2021).
- [51] E. Bauer and M. Sigrist, *Non-Centrosymmetric Superconductors: Introduction and Overview*, Vol. 847 (Springer, Berlin, 2012).
- [52] K. Shigeta, S. Onari, and Y. Tanaka, Superconducting pairing symmetry on the extended Hubbard model in the presence of the Rashba-type spin-orbit coupling, *J. Phys. Soc. Jpn.* **82**, 014702 (2013).
- [53] Y. Fujimoto, K. Miyake, and H. Matsuura, Deformation of the Fermi surface and anomalous mass renormalization by critical spin fluctuations through asymmetric spin-orbit interaction, *J. Phys. Soc. Jpn.* **84**, 043702 (2015).
- [54] D. Maruyama and Y. Yanase, Electron correlation effects in non-centrosymmetric metals in the weak coupling regime, *J. Phys. Soc. Jpn.* **84**, 074702 (2015).
- [55] A. Greco and A. P. Schnyder, Mechanism for Unconventional Superconductivity in the Hole-Doped Rashba-Hubbard Model, *Phys. Rev. Lett.* **120**, 177002 (2018).
- [56] X. Lu and D. S en echal, Parity-mixing superconducting phase in the Rashba-Hubbard model and its topological properties from dynamical mean-field theory, *Phys. Rev. B* **98**, 245118 (2018).
- [57] R. Ghadimi, M. Kargarian, and S. A. Jafari, Competing superconducting phases in the interacting two-dimensional electron gas with strong Rashba spin-orbit coupling, *Phys. Rev. B* **99**, 115122 (2019).
- [58] A. Greco, M. Bejas, and A. P. Schnyder, Ferromagnetic fluctuations in the Rashba-Hubbard model, *Phys. Rev. B* **101**, 174420 (2020).
- [59] K. Nogaki and Y. Yanase, Strongly parity-mixed superconductivity in the Rashba-Hubbard model, *Phys. Rev. B* **102**, 165114 (2020).
- [60] S. Wolf and S. Rachel, Spin-orbit coupled superconductivity: Rashba-Hubbard model on the square lattice, *Phys. Rev. B* **102**, 174512 (2020).
- [61] M. J. Trott and C. A. Hooley, Mixed-parity superconductivity near Lifshitz transitions in strongly spin-orbit-coupled metals, *Phys. Rev. Res.* **2**, 013106 (2020).
- [62] R. Soni, A. B. Sanyal, N. Kaushal, S. Okamoto, A. Moreo, and E. Dagotto, Multitude of topological phase transitions in bipartite Dice and Lieb lattices with interacting electrons and Rashba coupling, *Phys. Rev. B* **104**, 235115 (2021).
- [63] M. Biderang, M.-H. Zare, and J. Sirker, Proximity-driven ferromagnetism and superconductivity in the triangular Rashba-Hubbard model, *Phys. Rev. B* **105**, 064504 (2022).
- [64] N. E. Bickers and S. R. White, Conserving approximations for strongly fluctuating electron systems. II. Numerical results and parquet extension, *Phys. Rev. B* **43**, 8044 (1991).
- [65] N. Bulut, D. J. Scalapino, and S. R. White, Comparison of Monte Carlo and diagrammatic calculations for the two-dimensional Hubbard model, *Phys. Rev. B* **47**, 2742 (1993).
- [66] N. Bulut, D. J. Scalapino, and S. R. White, Effective particle-particle interaction in the two-dimensional Hubbard model, *Phys. Rev. B* **47**, 6157 (1993).
- [67] N. Bulut, D. J. Scalapino, and S. R. White, Spin-fluctuation mediated interaction in the two-dimensional Hubbard model, *Physica C: Superconductivity* **246**, 85 (1995).
- [68] N. Bulut, $d_{x^2-y^2}$ superconductivity and the Hubbard model, *Adv. Phys.* **51**, 1587 (2002).
- [69] H. Watanabe and Y. Yanase, Group-theoretical classification of multipole order: Emergent responses and candidate materials, *Phys. Rev. B* **98**, 245129 (2018).
- [70] S. Hayami, M. Yatsushiro, Y. Yanagi, and H. Kusunose, Classification of atomic-scale multipoles under crystallographic point groups and application to linear response tensors, *Phys. Rev. B* **98**, 165110 (2018).
- [71] M. Yatsushiro, H. Kusunose, and S. Hayami, Multipole classification in 122 magnetic point groups for unified understanding of multiferroic responses and transport phenomena, *Phys. Rev. B* **104**, 054412 (2021).
- [72] S. Sumita and Y. Yanase, Superconductivity in magnetic multipole states, *Phys. Rev. B* **93**, 224507 (2016).
- [73] Y. Yanase, FFLO superconductivity near the antiferromagnetic quantum critical point, *J. Phys. Soc. Jpn.* **77**, 063705 (2008).
- [74] K. Momma and F. Izumi, *VESTA3* for three-dimensional visualization of crystal, volumetric and morphology data, *J. Appl. Crystallogr.* **44**, 1272 (2011).